Resonance Raman Studies of Nickel Tetrathiolates and Nickel-Substituted Rubredoxins and Desulforedoxin

Yun-Hua Huang,[†] Isabel Moura,[‡] José J. G. Moura,[‡] Jean LeGall,[§] Jae-Bum Park,[§] Michael W. W. Adams,[§] and Michael K. Johnson*,[†]

Departments of Chemistry and Biochemistry and Center for Metalloenzyme Studies, University of Georgia, Athens, Georgia 30602, and Centro de Tecnologia Quimica e Biológica and Universidade Nova de Lisboa, Oeiras, Portugal

Received June 19, 1992

Low-temperature resonance Raman spectroscopy has been used to investigate the nickel coordination geometry in the $[Ni(SPh)_4]^{2-}$ anion in solution, Ni(II)-substituted rubredoxins from *Desulfovibrio gigas* and *Pyrococcus furiosus*, and Ni(II)-substituted desulforedoxin from *D. gigas*. Ni–S vibrational modes have been assigned on the basis of $^{58}Ni/^{60}Ni$ isotope shifts, polarization studies, and comparison with structurally characterized tetrathiolate Ni(II) complexes. The results indicate tetragonally elongated tetrahedral $[NiS_4]$ cores in the $[Ni(SPh)_4]^{2-}$ anion in solution and in both Ni(II)-rubredoxins and a distorted square planar $[NiS_4]$ core in Ni(II)-desulforedoxin. Cysteine deformation modes that are enhanced via coupling with Ni–S stretching modes are observed near 400 cm^{-1} in the spectra of both native and Ni(II)-substituted rubredoxins. The potential of resonance Raman for investigating Ni–cysteinate centers in other metalloproteins and for elucidating the conformation of coordinating cysteine residues is discussed in light of these new results.

Introduction

Interest in the chemistry and properties of nickel thiolates has been stimulated by the biological importance of nickel–thiolate coordination. X-ray absorption studies have established indigenous sulfur coordination for the active-site nickel centers in hydrogenases[1] and CO dehydrogenases,[2] and exogenous thiolates inhibit ureases by binding to the active-site binuclear nickel center.[3] In addition cysteinate-coordinated Zn(II) centers in several metalloproteins, e.g. metallothionein,[4] alcohol dehydrogenase,[5] and aspartate transcarbamoylase,[6] have been substituted by Ni(II) in order to elucidate structural properties of the metal binding site via the informative magnetic and electronic properties of Ni(II).

Resonance Raman spectroscopy has assumed an important role in the structural characterization of the metal centers in blue copper and iron–sulfur proteins via excitation into sulfur → metal charge-transfer bands. However, a similar role for resonance Raman in relation to cysteinate-coordinated biological nickel centers has yet to emerge. Preliminary resonance Raman spectra for Ni(II)-substituted azurin,[7] stellacyanin,[8] and liver alcohol dehydrogenase[9] have been reported, but the limited assignments must be viewed as extremely tentative in view of the extent and quality of the data. As a further step toward using resonance Raman spectroscopy to characterize biological nickel–cysteinate centers, we report here Ni–S vibrational assignments for two crystallographically-defined $[Ni(SPh)_4]^{2-}$ analog complexes, Ni(II)-substituted rubredoxins from *Desulfovibrio gigas* and *Pyrococcus furiosus* and Ni(II)-substituted desulforedoxin from *D. gigas*. The results demonstrate the potential of resonance Raman spectroscopy for determining the coordination geometry of biological Ni(II) centers with cysteine-rich coordination environments.

Experimental Section

Preparation of Compounds. $(Et_4N)_2[Ni(SPh)_4]$ and $(PPh_4)_2[Ni(SPh)_4]$ were prepared by following the published procedures, under an atmosphere of dry argon in a Vacuum Atmospheres glovebox (<1 ppm O_2).[10,11] Solutions in dry acetonitrile are stable in the presence of a 10-fold excess KSPh and were prepared and handled anaerobically under argon. Sample concentrations were based on ϵ_{680} = 327 M^{-1} cm^{-1}.[12] Rubredoxins from *D. gigas*,[13] *P. furiosus*,[14] and *Desulfovibrio desulfu-*

[†] Department of Chemistry and Center for Metalloenzyme Studies, University of Georgia.
[‡] Centro de Tecnologia Quimica e Biológica and Universidade Nova Lisboa.
[§] Department of Biochemistry and Center for Metalloenzyme Studies, University of Georgia.

(1) (a) Maroney, M. J.; Colpas, G. J.; Bagyinka, C. *J. Am. Chem. Soc.* **1990**, *112*, 7067. (b) Maroney, M. J.; Colpas, G. J.; Bagyinka, C.; Baidya, N.; Mascharak, P. K. *J. Am. Chem. Soc.* **1991**, *113*, 3962. (c) Scott, R. A.; Wallin, S. A.; Czechowski, M.; DerVartanian, D. V.; LeGall, J.; Peck, H. D., Jr.; Moura, I. *J. Am. Chem. Soc.* **1984**, *106*, 6864. (d) Eidsness, M. K.; Sullivan, R. J.; Scott, R. A. In *The Bioinorganic Chemistry of Nickel*; Lancaster, J. R., Ed.; VCH Publishers: New York, 1988; Chapter 4. (e) Eidsness, M. K.; Scott, R. A.; Prickril, B. C.; DerVartanian, D. V.; LeGall, J.; Moura, I.; Moura, J. G. G.; Peck, H. D., Jr. *Proc. Natl. Acad. Sci. U.S.A.* **1989**, *86*, 147. (f) Lindahl, P. A.; Kojima, N.; Hausinger, R. P.; Fox, J. A.; Teo, B. K.; Walsh, C. T.; Orme-Johnson, W. H. *J. Am. Chem. Soc.* **1984**, *106*, 3062.
(2) (a) Bastian, N. R.; Diekert, G.; Niederhoffer, E. C.; Teo, B.-K.; Walsh, C. T.; Orme-Johnson, W. H. *J. Am. Chem. Soc.* **1988**, *110*, 5581. (b) Cramer, S. P.; Eidsness, M. K.; Pan, W.-H.; Morton, T. A.; Ragsdale, S. W.; DerVartanian, D. V.; Ljungdahl, L. G.; Scott, R. A. *Inorg. Chem.* **1987**, *26*, 2477. (c) Tan, G. O.; Ensign, S. A.; Ciurli, S.; Scott, M. J.; Hedman, B.; Holm, R. H.; Ludden, P. W.; Korszun, Z. R.; Stephens, P. J.; Hodgson, K. O. *Proc. Natl. Acad. Sci. U.S.A.* **1992**, *89*, 4427.
(3) (a) Clark, P. A.; Wilcox, D. E. *Inorg. Chem.* **1989**, *28*, 1326. (b) Clark, P. A.; Wilcox, D. E.; Scott, R. A. *Inorg. Chem.* **1990**, *29*, 581. (c) Finnegan, M. G.; Kowal, A. T.; Werth, M. T.; Clark, P. A.; Wilcox, D. E.; Johnson, M. K. *J. Am. Chem. Soc.* **1991**, *113*, 4030.
(4) Vasak, M.; Kägi, J. H. R.; Holmquist, B.; Vallee, B. L. *Biochemistry* **1981**, *20*, 6659.
(5) (a) Formicka-Kozlowska, G.; Zeppezauer, M. *Inorg. Chim. Acta* **1988**, *151*, 183. (b) Dietrich, H.; Maret, W.; Kozlowski, H.; Zeppezauer, M. *J. Inorg. Biochem.* **1981**, *14*, 297.
(6) Johnson, R. S.; Schachman, H. K. *Proc. Natl. Acad. Sci. U.S.A.* **1980**, *77*, 1995.
(7) Ferris, N. S.; Woodruff, W. H.; Tennett, D. L.; McMillin, D. R. *Biochem. Biophys. Res. Commun.* **1979**, *88*, 288.
(8) Musci, G.; Desideri, A.; Morpurgo, L.; Tosi, L. *J. Inorg. Biochem.* **1985**, *23*, 93.
(9) (a) Maret, W.; Zeppezauer, M.; Sanders-Loehr, J.; Loehr, T. M. *Biochemistry* **1983**, *22*, 3202. (b) Maret, W.; Shienke, A. K.; Wheeler, W. D.; Loehr, T. M.; Sanders-Loehr, J. *J. Am. Chem. Soc.* **1986**, *108*, 6351.
(10) Yamamura, T.; Miyamae, H.; Katayama, Y.; Sasaki, Y. *Chem. Lett.* **1985**, 269.
(11) Rosenfield, S. G.; Armstrong, W. H.; Mascharak, P. K. *Inorg. Chem.* **1986**, *25*, 3014.
(12) Holah, D. G.; Coucouvanis, D. *J. Am. Chem. Soc.* **1975**, *97*, 6917.
(13) Moura, I.; Bruschi, M.; LeGall, J.; Moura, J. J. G.; Xavier, A. V. *Biochem. Biophys. Res. Commun.* **1977**, *75*, 1037.

0020-1669/93/1332-0406$04.00/0

ricans (ATCC 27774)[15] and desulforedoxin from *D. gigas*[16] were purified as previously described. Formation of the apoprotein and subsequent reconstitution with Ni(II) was performed using the method of Moura et al.[17] Sample concentrations were assessed on the basis of the extinction coefficients reported for *D. gigas* Ni(II)-rubredoxin and Ni(II)-desulforedoxin.[17]

^{60}Ni- and ^{58}Ni-isotopically labeled complexes and *P. furiosus* Ni(II)-rubredoxin were prepared using ^{58}Ni metal powder (99.66% enrichment, Oakridge National Laboratory) or ^{60}Ni metal powder (99.65% enrichment, Oakridge National Laboratory) after dissolving the metal in warm concentrated HCl and evaporation to yield light green crystals of $^{58}NiCl_2 \cdot 6H_2O$ or $^{60}NiCl_2 \cdot 6H_2O$.

Physical Measurements. UV–visible absorption spectra were measured in 0.1-cm cuvettes using a Hewlett Packard 8452A diode array spectrophotometer interfaced to an IBM PC-XT microcomputer. Raman spectra were recorded using an Instruments SA Ramanor U1000 spectrometer fitted with a cooled RCA 31034 photomultiplier tube with 90° scattering geometry, using lines from a Coherent Innova 100-10 argon ion or 200-K2 krypton ion laser. Plasma lines were removed using a Pellin Broca Prism premonochromator, and laser powers at the sample were between 20 and 80 mW. Samples were placed on the end of a cold finger of an Air Products Displex Model CSA-202E closed-cycle refrigerator using a custom-designed anaerobic sample holder.[18] This enables samples to be cooled down to 17 K, which results in improved spectral resolution and prevents laser-induced sample degradation. For proteins and solutions of inorganic complexes, about 10 μL of a concentrated solution (2–5 mM) was placed on the gold-plated sample holder. Solid-state spectra were obtained by grinding up crystalline complexes with KBr (5% w/w) and pressing a pellet in the glovebox. The resulting pellet was adhered to the sample holder using crycon grease which contains finely divided copper for good thermal contact.

Raman spectra were recorded digitally using photon counting electronics interfaced to an IBM PC-XT microcomputer. Improvements in signal to noise were achieved by multiple scanning; no smoothing function was applied to the data. Typically, each spectrum is the sum of 4–20 scans, each involving photon counting for 1 s every 0.2 cm^{-1}, with 6-cm^{-1} spectral resolution. Bands originating from the frozen buffer solution, normalized to the intensity of the ice band at 230 cm^{-1}, and a linear ramp due to the underlying fluorescence background have been subtracted from the spectra of Ni(II)-rubredoxins and Ni(II)-desulforedoxin. Band positions were calibrated using the excitation frequency and the principal bands of CCl_4 and are accurate to ±1 cm^{-1}. ^{58}Ni/^{60}Ni isotope shifts were obtained by alternately collecting spectra from isotopically labeled samples on the same sample probe, with calibration checks after each scan, and are accurate to ±0.2 cm^{-1}. Isotope shifts were calculated from the ^{60}Ni minus ^{58}Ni difference spectra using the published procedure.[19]

Results and Discussion

The Ni–S normal vibrational modes associated with a tetrahedral $[NiS_4]$ unit are shown in Figure 1. All four modes are Raman active and based on extensive vibrational studies of metal tetrahalogen anions; the expected order of frequencies is $\nu(T_2)$ Ni–S > $\nu(A_1)$ Ni–S > $\delta(T_2)$ S–Ni–S > $\delta(E)$ S–Ni–S.[20] Lowering the symmetry to D_{2d} via a tetragonal compression or elongation removes the E and T_2 modes resulting in $A_1 + B_1$ and $B_2 + E$ modes, respectively. For a tetragonal elongation, the E mode is expected to occur at lower energy than the B_2 mode, and vice versa for a tetragonal compression.[21] Further lowering of the symmetry from idealized D_{2d} symmetry can result in splitting of the degenerate E modes. Square planar is the alternative idealized geometry for a $[NiS_4]$ unit, and the normal vibrational modes associated with this coordination arrangement are also depicted in Figure 1. Under rigorous D_{4h} symmetry only the centrosymmetric modes designated by a g subscript are Raman active. However, a rigorous inversion center is extremely unlikely for the low-symmetry coordination environments generally encountered for biological metal centers, and noncentrosymmetric modes designated by a u subscript are expected to be observable in the Raman spectrum. The expected order of Ni–S stretching frequencies is $\nu(E_u)$ Ni–S > $\nu(A_{1g})$ Ni–S > $\nu(B_{2g})$ Ni–S with the in-plane and out-of-plane deformations occurring at significantly lower energies.[20] The degeneracy of the highest energy Ni–S stretching mode will be removed by low-symmetry distortions.

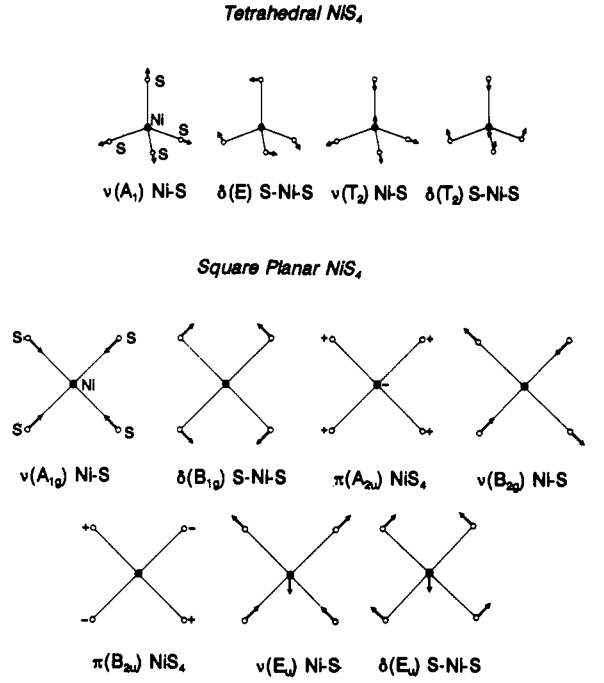

Figure 1. Vibrational modes for tetrahedral and square planar $[NiS_4]$ cores.

$[Ni(SPh)_4]^{2-}$. Crystallographically defined salts involving the $[Ni(SPh)_4]^{2-}$ anion provide an appropriate starting point for investigating the vibrational characteristics of distorted tetrahedral $[NiS_4]$ cores in biological systems. In almost all $[M(SPh)_4]^{2-,-}$ complexes, the phenyl ring is coplanar with the M–S–C plane in order to facilitate overlap of the 3pπ sulfur orbital with the aromatic ring, and the coplanar [M–S–Ph] unit is approximately perpendicular to and bisecting a face of the MS_4 tetrahedron.[22,23] Given these requirements, only two conformational isomers are possible for the $[M(SPh)_4]$ unit: S_4 and D_{2d} isomers, which are predicted to have tetragonally compressed and elongated $[MS_4]$ cores, respectively.[22-24] Both types of isomer can be obtained for $[Ni(SPh)_4]^{2-}$ depending on the nature of the counterion. In the case of the $[PPh_4]^+$ salt, the $[Ni(SPh)_4]^{2-}$ anion has *approximate* D_{2d} symmetry with a tetragonally elongated $[NiS_4]$ core (Ni–S bond lengths equal to 2.272, 2.287, 2.289, and 2.303 Å; S–Ni–S bond angles equal to 92.0, 92.7, 115.4, 116.3, 117.9, and 124.9°).[22] In contrast, for the $[NEt_4]^+$ salt, the $[Ni(SPh)_4]^{2-}$ anion has

(14) Blake, P. R.; Park, J.-B.; Bryant, F. O.; Aono, S.; Magnuson, J. K.; Eccleston, E.; Howard, J. B.; Summers, M. F.; Adams, M. W. W. *Biochemistry* **1991**, *30*, 10885.
(15) Hormel, S.; Walsh, K. A.; Prickril, B. C.; Titani, K.; LeGall, J.; Sieker, L. C. *FEBS Lett.* **1986**, *201*, 147.
(16) (a) Moura, I.; Bruschi, M.; LeGall, J.; Moura, J. J. G.; Xavier, A. V. *Biochem. Biophys. Res. Commun.* **1977**, *75*, 1037. (b) Moura, I.; Huynh, B. H.; Hausinger, R. P.; LeGall, J.; Xavier, A. V.; Münck, E. *J. Biol. Chem.* **1980**, *255*, 2493.
(17) Moura, I.; Teixeira, M.; LeGall, J.; Moura, J. J. G. *J. Inorg. Biochem.* **1991**, *44*, 127.
(18) Drozdzewski, P. M.; Johnson, M. K. *Appl. Spectrosc.* **1988**, *42*, 1575.
(19) Shelnutt, J. A.; Rousseau, D. L.; Dethemers, J. K.; Margoliash, E. *Proc. Natl. Acad. Sci. U.S.A.* **1979**, *76*, 3865.
(20) Nakamoto, K. *Infrared and Raman Spectra of Inorganic and Coordination Compounds*, 4th ed.; Wiley-Interscience: New York, 1986.
(21) (a) Yachandra, V. K.; Hare, J.; Moura, I.; Spiro, T. G. *J. Am. Chem. Soc.* **1983**, *105*, 6455. (b) Czernuszewicz, R. S.; LeGall, J.; Moura, I.; Spiro, T. G. *Inorg. Chem.* **1986**, *25*, 696.
(22) Swenson, D.; Baenziger, N. C.; Coucouvanis, D. *J. Am. Chem. Soc.* **1978**, *100*, 1932.
(23) Silver, A.; Koch, S. A.; Millar, M. *Inorg. Chem.*, in press.
(24) Koch, S. A.; Maelia, L. E.; Millar, M. *J. Am. Chem. Soc.* **1983**, *105*, 5944.

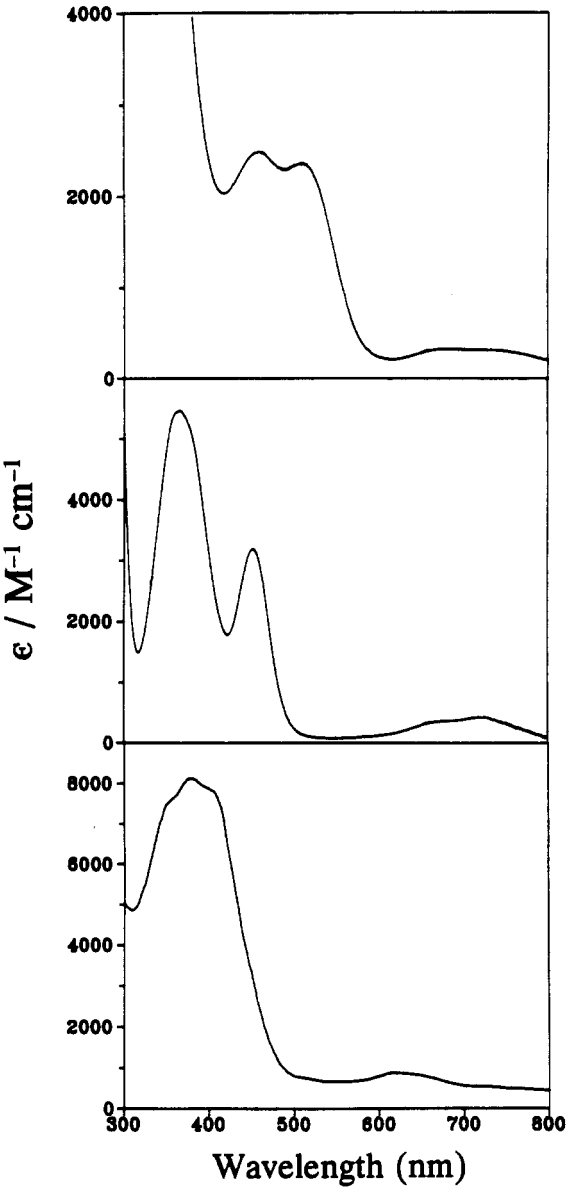

Figure 2. UV–visible absorption spectra of $[Ni(SPh)_4]^{2-}$ and Ni(II)-rubredoxin and desulforedoxin. Upper panel: $(PPh_4)_2[Ni(SPh)_4]$, 2 mM in acetonitrile solution with a 10-fold excess of KSPh. Middle panel: *P. furiosus* Ni(II)-rubredoxin, 0.4 mM in 100 mM Tris-HCl buffer, pH 7.8. Lower panel: *D. gigas* Ni(II)-desulforedoxin, 0.3 mM in 100 mM Tris-HCl buffer, pH 7.8.

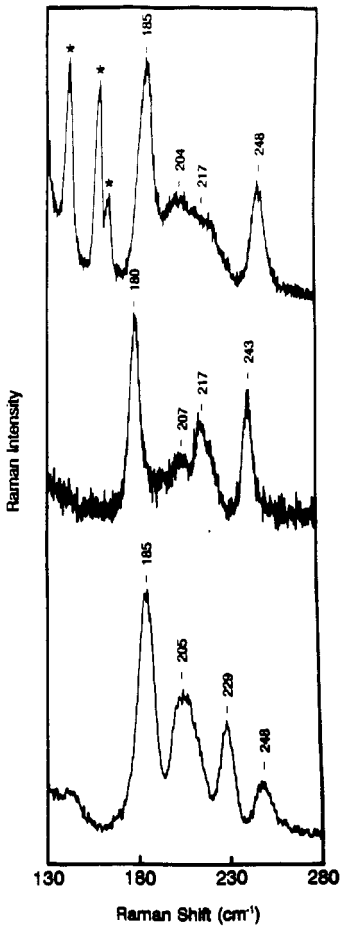

Figure 3. Comparison of the solid-state and solution resonance Raman spectra of $[Ni(SPh)_4]^{2-}$ in the Ni–S stretching region. Upper spectrum: $(PPh_4)_2[Ni(SPh)_4]$ (5 mM) in acetonitrile solution (10-fold excess of KSPh) with 488.0-nm excitation and 4-cm^{-1} spectral resolution. Bands labeled with an asterisk arise from acetonitrile. Middle spectrum: $(PPh_4)_2[Ni(SPh)_4]$ in the solid state (5% w/w in KBr) with 488.0-nm laser excitation and 4-cm^{-1} spectral resolution. Lower spectrum: $(NEt_4)_2[Ni(SPh)_4]$ in solid state (5% w/w in KBr) with 476.5-nm laser excitation and 6-cm^{-1} spectral resolution. The spectra were recorded at 17 K and are the sum of 22, 8, and 4 scans for the upper, middle, and lower spectra, respectively. Each scan involved photon counting for 1.0 s at 0.2-cm^{-1} increments.

approximate S_4 symmetry with a tetragonally compressed $[NiS_4]$ core (Ni–S bond lengths equal to 2.279, 2.287, 2.296, and 2.306 Å; S–Ni–S bond angles equal to 97.2, 104.4, 105.2, 109.1, 118.6, and 123.7°).[10] Solutions of both salts in CH_3CN in the presence of excess KSPh exhibited identical UV–visible absorption spectra, consisting of a broad d–d band centered around 700 nm and two intense S → Ni(II) charge-transfer bands centered at 460 and 510 nm; see Figure 2. Laser excitation within the charge-transfer envelope of bands should therefore be effective in enhancing Ni–S vibrational modes. Hence the initial objectives of this work were to determine if the two structural forms of $[Ni(SPh)_4]^{2-}$ in the solid state have distinct resonance Raman spectra and, this being so, to use resonance Raman to assess the structure of the anion in solution.

Resonance Raman spectra in the Ni–S stretching region for $(PPh_4)_2[Ni(SPh)_4]$ and $(NEt_4)_2[Ni(SPh)_4]$ in the solid state and $[Ni(SPh)_4]^{2-}$ in CH_3CN solution are shown in Figure 3. Identical solution spectra were observed irrespective of whether $(PPh_4)_2[Ni(SPh)_4]$ or $(NEt_4)_2[Ni(SPh)_4]$ was used. Above 300 cm^{-1} the spectra are dominated by bands associated with the benzenethiolate ligands (spectra not shown). With the exception of the solvent bands marked with asterisks, the bands observed in the 130–280-cm^{-1} region were assigned to Ni–S stretching modes on the basis of the $^{58}Ni/^{60}Ni$ isotope shifts and parallel Raman studies of KSPh, CH_3CN, PPh_4Cl, and NEt_4Cl which were used to assess contributions from counterions, solvent, or excess KSPh; see Table I.

Figure 4 shows solid-state spectra obtained with 514.5-nm excitation for $(PPh_4)_2[Ni(SPh)_4]$ that has been isotopically labeled with ^{60}Ni and ^{58}Ni and the ^{60}Ni minus ^{58}Ni difference spectrum. Clear $^{58}Ni/^{60}Ni$ isotope shifts are observed for the bands that occur at 207, 217, and 243 cm^{-1} in the natural abundance samples. Analysis of the difference spectrum[19] indicates that each of these bands is upshifted by 1.4 cm^{-1} in the ^{58}Ni spectrum. Accordingly they are assigned to components of the asymmetric $\nu(T_2)$ Ni–S stretching mode. The totally symmetric $\nu(A_1)$ Ni–S stretching mode is expected to lower energy and is readily assigned to the band at 180 cm^{-1} in view of its intensity and negligible $^{58}Ni/^{60}Ni$ isotope shift. Further support for this assignment comes from polarization studies which showed the 180-cm^{-1} band to be much more polarized than the bands at 207, 217, or 243 cm^{-1}. Although polarization studies on frozen-solution or solid-state samples are problematical due to depolarization of the scattered light via multiple reflections, they can be used to give a qualitative

Table I. Ni–S Vibrational Frequencies (cm^{-1}), $^{58}Ni/^{60}Ni$ Isotope Shifts, and Assignments for $[Ni(SPh)_4]^{2-}$ and Ni(II)-Rubredoxins

	$[Ni(SPh)_4]^{2-}$ [b]			Ni(II)-rubredoxin[b]	
assgnt[a]	$[PPh_4]^+$ salt	$[NEt_4]^+$ salt	CH_3CN soln	*P. furiosus*	*D. gigas*
δ(E)(S–Ni–S)				126 (1.2)	128
$\delta(T_2)$(S–Ni–S) or δ(Ni–S–C)	120 (1.0)	120 (1.0)		171 (1.6)	174
				203 (1.8)	185
$\nu(A_1)$(Ni–S)	180 (0.0)	185 (0.0)	185	239 (0.0)	236
$\nu(T_2)$(Ni–S)	207 (1.4)	205 (1.5)	204	294 (2.2)	302
	217 (1.4)	229 (1.5)	217	294 (2.2)	302
	243 (1.4)	248 (1.2)	248	335 (3.2)	337
δ(Cys)[c]				397 (0.0)	399
				415 (0.0)	418

[a] Under parent T_d symmetry for $[NiS_4]$ core. [b] ^{58}Ni minus ^{60}Ni frequency shifts are given in parentheses. [c] Internal bending or torsional modes of coordinated cysteine residue(s).

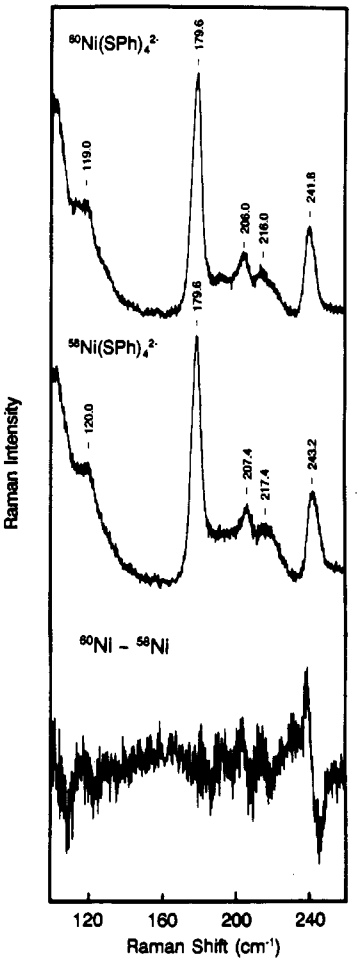

Figure 4. $^{58}Ni/^{60}Ni$ isotope shifts for $(PPh_4)_2[Ni(SPh)_4]$. Upper spectrum: $(PPh_4)_2[^{60}Ni(SPh)_4]$. Middle spectrum: $(PPh_4)_2[^{58}Ni(SPh)_4]$. Lower spectrum: ^{60}Ni minus ^{58}Ni difference spectrum. Spectra were recorded at 17 K with 514.5-nm laser excitation and 6-cm^{-1} spectral resolution for solid-state samples (5% in w/w KBr). The spectra are the sum of four scans with each scan involving photon counting for 0.5 s at 0.2-cm^{-1} increments.

assessment of the polarization of the scattered light in strongly absorbing samples.[25]

Similar $^{58}Ni/^{60}Ni$ isotope shift data were observed for solid-state samples of $(NEt_4)_2[Ni(SPh)_4]$; see Table I. In this case the $\nu(A_1)$ Ni–S stretching mode occurs at 185 cm^{-1}, and the components of the $\nu(T_2)$ Ni–S stretching mode are observed at 205, 229, and 248 cm^{-1}. Clearly the two structural forms of the $[Ni(SPh)_4]^{2-}$ anion that occur in the solid state have distinct Raman spectra in the Ni–S stretching region and the frequencies of $\nu(T_2)$ components are readily rationalized in terms of the crystal structures under effective D_{2d} symmetry for the $[NiS_4]$ core. For the tetragonally elongated $[NiS_4]$ core in $(PPh_4)_2[Ni(SPh)_4]$, the 207- and 217-cm^{-1} bands are assigned to components of lower energy E mode and the 243-cm^{-1} band to the higher energy B_2 mode. The tetragonally compressed $[NiS_4]$ core in $(NEt_4)_2[Ni(SPh)_4]$ is less symemtrical, and hence a larger splitting of the higher energy E mode is anticipated. Consequently the 205-cm^{-1} band is assigned to the B_2 mode, and the 229- and 248-cm^{-1} bands are assigned to components of the E mode.

The resonance Raman spectrum of $[Ni(SPh)_4]^{2-}$ in acetonitrile solution is most similar to that of $(PPh_4)_2[Ni(SPh)_4]$ and is consistent with a tetragonally elongated $[NiS_4]$ core. Under effective D_{2d} symmetry, the dominant 185-cm^{-1} band is assigned to $\nu(A_1)$ Ni–S stretching, the 204- and 217-cm^{-1} bands are assigned to components of the $\nu(E)$ Ni–S stretching mode, and the 248-cm^{-1} band is assigned to the $\nu(B_2)$ Ni–S stretching mode. The separation of the E and B_2 modes in solution, 37 cm^{-1}, is larger than that for $(PPh_4)_2[Ni(SPh)_4]$ in the solid state, 31 cm^{-1}, suggesting a greater tetragonal distortion in solution. We conclude that, although crystal packing forces dictate the sign and can modulate the magnitude of the axial distortion, they are not responsible for the distortion. Rather a tetragonally distorted $[NiS_4]$ core is an intrinsic property of the $[Ni(SPh)_4]^{2-}$ anion.

A tetragonally elongated structure in solution is also consistent with the electronic ground- and excited-state properties. Variable-temperature MCD studies of $[Ni(SPh)_4]^{2-}$ in a 50/50 DMF/toluene glass indicate a zero-field split $^3A_2$ ground state that arises from a tetragonal elongation of the parent $^3T_1$ ground state under T_d symmetry.[26] Likewise the splitting of the highest energy d–d band is attributed to tetragonal distortion of the parent $^3T_1$(P) excited state, resulting in well-resolved $^3A_2 \rightarrow {}^3A_2$ and $^3A_2 \rightarrow {}^3E$ transitions.[26]

Identification and assignment of the bending modes of the $[NiS_4]$ core in $[Ni(SPh)_4]^{2-}$ has been limited by intense Rayleigh scattering for solid-state samples and by strong solvent bands in solution samples. A weak band at 120 cm^{-1} with a 1.0-cm^{-1} $^{58}Ni/^{60}Ni$ isotope shift is observed in the solid-state spectra of both $(PPh_4)_2[Ni(SPh)_4]$ and $(NEt_4)_2[Ni(SPh)_4]$ and is tentatively assigned to a component of the $\delta(T_2)$ S–Ni–S bending mode.

Ni(II)-Rubredoxin. Ni(II)-rubredoxins from *D. gigas* and *P. furiosus* exhibit almost identical UV–visible absorption spectra. The S → Ni(II) charge-transfer transitions are blue shifted, compared to those of $[Ni(SPh)_4]^{2-}$, and are assigned to well-resolved bands center at 360 and 450 nm, while the highest energy d–d band remains centered around 700 nm; see Figure 2. Using

(25) (a) Spaulding, L. D.; Change, C. C.; Yu, N.-T.; Felton, R. H. *J. Am. Chem. Soc.* **1975**, *97*, 2517. (b) Strommen, D. P.; Bajdor, K.; Czernuszewicz, R. S.; Blinn, E. L.; Nakamoto, K. *Inorg. Chim. Acta* **1982**, *63*, 151. (c) Moulis, J.-M.; Meyer, J.; Lutz, M. *Biochemistry* **1984**, *23*, 6605.

(26) Kowal, A. T.; Zambrano, I. C.; Moura, I.; Moura, J. J. G.; LeGall, J.; Johnson, M. K. *Inorg. Chem.* **1988**, *27*, 1162. In Figure 7 of this paper, the abscissa should read increasing tetragonal elongation rather than increasing tetragonal compression.

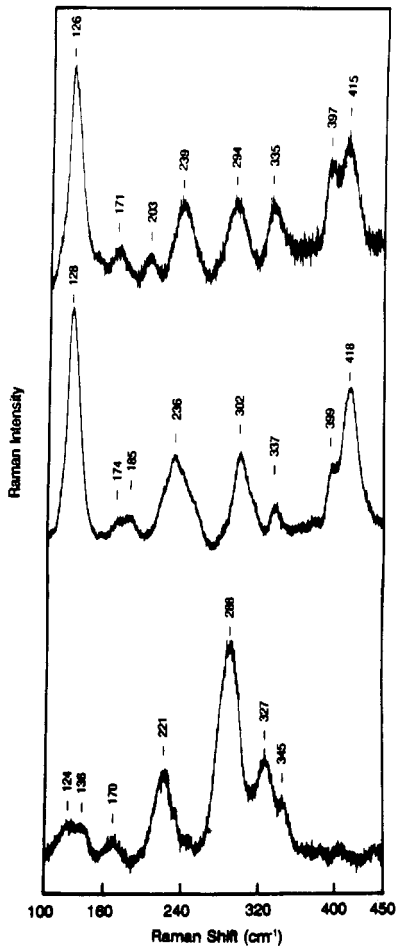

Figure 5. Resonance Raman spectra for Ni(II)-rubredoxins from *P. furiosus* (upper spectrum) and *D. gigas* (middle spectrum) and Ni(II)-desulforedoxin from *D. gigas* (lower spectrum). The spectra were recorded at 17 K with 6-cm^{-1} spectral resolution using 457.9-nm excitation for the Ni(II)-rubredoxins and 406.7-nm excitation for Ni(II)-desulforedoxin. Samples were 2.5 mM (*D. gigas* rubredoxin and desulforedoxin) and 3 mM (*P. furiosus*) in 100 mM Tris-HCl buffer, pH 7.8. Bands originating from the frozen buffer solution have been subtracted. The rubredoxin spectra are the sum of 10 scans, and the desulforedoxin spectrum is the sum of 26 scans. Each scan involved photon counting for 1.0 s at 0.2-cm^{-1} increments.

the available lines from argon ion and krypton ion lasers in the range 406.7–530.9 nm, optimal resonance enhancement of Ni–S vibrational modes was observed with 457.9-nm excitation. Resonance Raman spectra for *D. gigas* and *P. furiosus* Ni(II)-rubredoxins in the range 100–450 cm^{-1}, obtained at this excitation wavelength, are shown in Figure 5. The frozen buffer solution has a pronounced band at 230 cm^{-1} and a weaker feature at 315 cm^{-1}. The former was apparent in the raw data as a shoulder on the bands centered at 239 and 236 cm^{-1} in *P. furiosus* and *D. gigas* Ni(II)-rubredoxins, respectively. The spectrum of the frozen buffer solution has been subtracted from those shown in Figure 5.

Vibrational assignments were facilitated by $^{58}Ni/^{60}Ni$ isotope shifts for *P. furiosus* Ni(II)-rubredoxin; see Figure 6. While the discussion below focuses on *P. furiosus* Ni(II)-rubredoxin, because of the availability of isotope shift data, the close similarity in terms of both band frequencies and relative intensities attests to very similar [NiS_4] sites and enables the assignments to be generalized to include *D. gigas* Ni(II)-rubredoxin; see Table I. On the basis of the ^{60}Ni minus ^{58}Ni difference spectrum, significant $^{58}Ni/^{60}Ni$ isotope shifts in the range 1.2–3.2 cm^{-1} are only observed for the bands at 335, 294, 203, 171, and 126 cm^{-1}. The bands at 415, 397, and 239 cm^{-1} show negligible isotope shifts. (In the case of the 239-cm^{-1} band, this is most apparent in overlays of

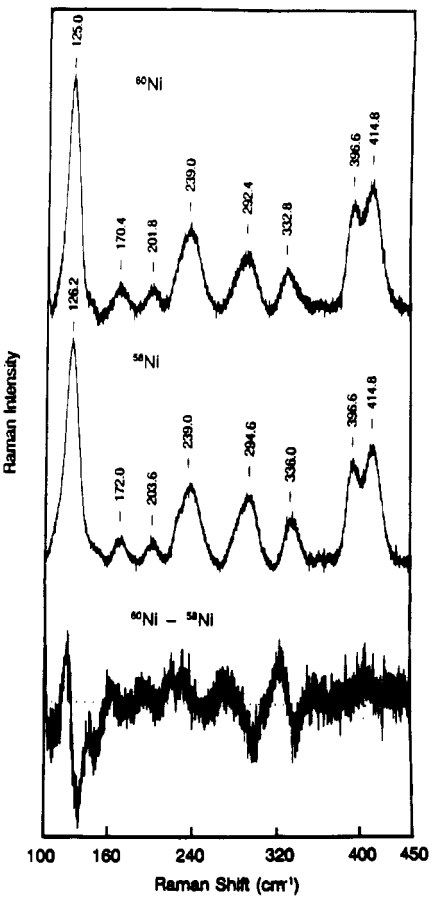

Figure 6. $^{58}Ni/^{60}Ni$ isotope shifts for Ni(II)-rubredoxin from *P. furiosus*. Upper spectrum: ^{60}Ni-rubredoxin. Middle spectrum: ^{58}Ni-rubredoxin. Lower spectrum: ^{60}Ni minus ^{58}Ni difference spectrum. Conditions are as for Figure 4, except that the ^{60}Ni sample was 4 mM and the spectrum is the sum of 26 scans and the ^{58}Ni sample was 3 mM and the spectrum is the sum of 13 scans.

the ^{58}Ni and ^{60}Ni spectra since the difference spectrum on the low energy side of this band is unreliable due to incomplete or oversubstraction of the ice band at 230 cm^{-1}.) With the exception of the bands at 415 and 397 cm^{-1}, the pattern of bands and their isotope shifts are consistent with vibrations of a tetragonally distorted [NiS_4] core. The $\nu(A_1)$ Ni–S stretching mode is assigned at 239 cm^{-1} in view of the lack of $^{58}Ni/^{60}Ni$ isotope shift. The two higher energy modes at 294 and 335 cm^{-1}, which have ^{58}Ni upshifts of 2.2 and 3.2 cm^{-1}, respectively, are therefore assigned to components of the $\nu(T_2)$ Ni–S stretching mode. As expected, the mass effect of the benzenethiolate results in much lower frequencies for the Ni–S stretching modes in $[Ni(SPh)_4]^{2-}$ compared to the corresponding modes in Ni(II)-rubredoxin; see Table I. In view of the breadth and asymmetry of the band centered at 294 cm^{-1}, this band is assigned to the E component with the 335-cm^{-1} band as the B_2 component under D_{2d}. This assignment dictates a tetragonal elongation which is consistent with the ground- and excited-state properties deduced from variable-temperature MCD studies of Ni(II)-rubredoxins from *D. gigas*[26] and *P. furiosus*.[27]

The lower energy modes at 203, 171, and 126 cm^{-1} exhibit ^{58}Ni upshifts of 1.8, 1.6, and 1.2 cm^{-1}, respectively, and are thus assigned to bending modes of the [NiS_4] core or Ni–S–C_β bending. Because of its intensity and small isotope shift, the 126-cm^{-1} band is tentatively assigned to the A_1 component of the $\delta(E)$ S–Ni–S bending mode under effective D_{2d} symmetry. The bands at 171 and 203 cm^{-1} are, therefore, tentatively assigned to components

(27) Huang, Y.-H.; Park, J.-B.; Adams, M. W. W.; Johnson, M. K. Unpublished results.

of the $\delta(T_2)$ S–Ni–S bending mode. However, assignment of one or both of these bands to Ni–S–C_β bending modes cannot be excluded.

The Ni–S stretching vibrations of the [NiS_4] core can all be accounted for without considering the bands at 397 and 415 cm^{-1} (399 and 418 cm^{-1} in *D. gigas* Ni(II)-rubredoxin). However, these bands are clearly associated with the Ni–S(Cys) unit since they undergo strong resonant enhancement with excitation into the S → Ni(II) charge-transfer band centered at 450 nm. By analogy with blue copper proteins which exhibit intense bands in the 350–450-cm^{-1} region,[28] they are assigned to cysteine deformation modes that become enhanced as a result of coupling with Ni–S stretching modes. The most obvious candidate is S–C_β–C_α bending since this mode is structurally forced to couple to Ni–S stretching. However, resonance Raman studies and normal mode calculations for Fe–S proteins and analog complexes suggest that the natural frequency of this bending mode is closer to 300 than 400 cm^{-1}.[21,29] Alternative possibilities are Ni–S–C_β–C_α torsional modes and C_β–C_α–N, C_β–C_α–CO, or N–C_α–CO bending modes of the coordinated cysteines or some combination thereof. These modes are expected in the 300–500-cm^{-1} region and could potentially be enhanced via coupling to Ni–S stretching modes.

Coupling of M–S stretching modes with the S–C_β–C_α bending modes of coordinated cysteine residues has been invoked extensively to explain the resonance Raman spectra of blue copper proteins,[28] native Fe rubredoxins,[21] and proteins containing [2Fe–2S] and [4Fe–4S] clusters.[29,30] Maximal coupling is expected when the M–S–C_β–C_α dihedral angle is close to 180° and minimal at 90 or 270°. In the case of native rubredoxins, the X-ray crystal structure data indicate two dihedral angles close to 180° and two close to 270°.[30] The near coincidence of the $\nu(A_1)$ Fe–S stretching and S–C_β–C_α bending frequencies combined with two dihedral angles close to 180° results in strong coupling of these modes. The consequence is that the S–C_β–C_α bending mode is strongly enhanced and is assigned to a pronounced shoulder at 324 cm^{-1} on the side of the intense $\nu(A_1)$ Fe–S stretching mode at 314 cm^{-1}. The lack of a band attributable to S–C_β–C_α bending in Ni(II)-rubredoxin most likely relates to the lower Ni–S stretching frequencies and hence weaker coupling of these two modes. It is conceivable that this mode is obscured by the bands at 294 and 335 cm^{-1} that are assigned to components of $\nu(T_2)$ Ni–S on the basis of the magnitude of their $^{58}Ni/^{60}Ni$ isotope shifts.

One puzzling aspect of the assignment of bands around 400 cm^{-1} in Ni(II)-rubredoxins and blue copper proteins to deformation modes of coordinated cysteine(s) that are dominated by internal coordinates other than S–C_β–C_α bending was that no equivalent bands have been reported for native rubredoxins. This prompted us to reinvestigate the resonance Raman spectra of some native rubredoxins and desulforedoxin. In all cases investigated thus far, bands between 400 and 420 cm^{-1} were observed in the low-temperature resonance Raman spectra, e.g. 418 cm^{-1} in *D. gigas* rubredoxin, 415 cm^{-1} in *D. gigas* desulforedoxin, 403 cm^{-1} in *P. furiosus* rubredoxin, and 400 and 414 cm^{-1} in *D. desulfuricans* (ATCC 27774) rubredoxin. These bands can be seen with excitations in the range 457.9–530.9 nm but are most apparent in spectra obtained with 457.9-nm excitation, where they exhibit intensities comparable to those of the $\nu(T_2)$ Fe–S bands. Although rigorous assignments are not presently available, it is clear that detailed rationalization of the cysteine deformation modes that become enhanced via coupling with M–S stretching modes is one of the most important objectives in resonance Raman studies of cysteinate-coordinated metal centers.

The vibrational and electronic data discussed above both indicate approximate D_{2d} symmetry for the [NiS_4] core in Ni(II)-rubredoxins. However, the NMR data for *D. gigas* Ni(II)-rubredoxin clearly demonstrate that this effective symmetry does not extend to the conformational arrangement of the S–C_β–C_α side chains of the coordinating cysteine residues.[17] Well-resolved contact-shifted resonances are observed from each of the cysteinyl protons; eight resonances in the range 150–370 ppm from the β-CH_2 protons and four resonances in the range 14–35 ppm from the α-CH protons.[17] Such a result is not surprising given the asymmetry of the protein environment and suggests differences in the conformations and/or H-bonding interactions for each of the ligating cysteine residues.

Ni(II)-Desulforedoxin. Desulforedoxin provides an interesting variant of the rubredoxin family of proteins. The arrangement of cysteine residues coordinating Fe in rubredoxins is highly conserved and involves two Cys–X–X–Cys sequences, one close to the N-terminus and the other close to the C-terminus.[14,31] In contrast, the coordinating cysteines in desulforedoxin are arranged in Cys–Cys and Cys–X–X–Cys sequences.[16] Although the available spectroscopic data indicate that distorted-tetrahedral cysteinate–Fe coordination is retained in desulforedoxin, the stereochemical constraints imposed by the anomalous cysteine sequence are responsible for differences in UV–visible absorption, EPR, Mössbauer, and resonance Raman spectra compared to rubredoxin.[16b,21a]

More dramatic differences between rubredoxin and desulforedoxin are apparent in the Ni(II)-substituted forms. As noted previously,[17] the UV–visible absorption spectra of Ni(II)-rubredoxin and desulforedoxin are quite distinct; see Figure 2. The highest energy d–d band is blue-shifted to 610 nm, and the S → Ni(II) charge-transfer region consists of three unresolved bands centered at 350, 375, and 405 nm. The blue-shift of the lowest energy charge-transfer band results in negligible resonant enhancement of Ni–S stretching modes with 457.9-nm excitation. High-quality spectra were, however, obtained at low temperatures with 406.7-nm excitation; see Figure 5.

The pattern of bands and frequencies for Ni(II)-desulforedoxin are completely different from those of Ni(II)-rubredoxin, suggesting a very different coordination geometry. Unfortunately this protein was not available in sufficient quantities to enable preparation of ^{58}Ni and ^{60}Ni labeled samples. However, tentative band assignments have been made based on comparison with the Raman spectrum of well-characterized Ni–thiolate complexes. By analogy with Ni(II)-rubredoxins, the bands at 221, 288, 327, and 345 cm^{-1} are assigned to Ni–S stretching modes. The intensity of the 288-cm^{-1} band suggests assignment to a totally symmetric Ni–S stretching mode. Therefore, contrary to tetrahedral coordination where the totally symmetric mode is lowest in energy among the Ni–S stretching modes, this mode appears to be flanked by asymmetric Ni–S stretching modes in Ni(II)-desulforedoxin. Such an arrangement is consistent with approximately square planar geometry for the cysteinyl S ligands. For example, consider the structurally characterized $[Ni(dto)_2]^{2-}$ anion (dto^{2-} is the dithiooxalate ion) which has a square planar NiS_4 unit. The IR and Raman spectra have been rigorously assigned on the basis of the $^{58}Ni/^{62}Ni$ isotope shifts and normal mode calculations.[32] The totally symmetric $\nu(A_{1g})$ Ni–S stretching band is observed

(28) (a) Nestor, L.; Larrabee, J. A.; Woolery, G.; Reinhammar, B.; Spiro, T. G. *Biochemistry* **1984**, *23*, 1084. (b) Blair, D. F.; Campbell, G. W.; Schoonover, J. R.; Chan, S. I.; Gray, H. B.; Malmstrom, B. G.; Pecht, I.; Swanson, B. I.; Woodruff, W. H.; Cho, W. K.; English, A. M.; Fry, H. A.; Lum, V.; Norton, K. A. *J. Am. Chem. Soc.* **1985**, *107*, 5755. (c) Han, J.; Adman, E. T.; Beppu, T.; Codd, R.; Freeman, H. C.; Huq, L.; Loehr, T. M.; Sanders-Loehr, J. *Biochemistry* **1991**, *30*, 10904.

(29) (a) Han, S.; Czernuszewicz, R. S.; Spiro, T. G. *J. Am. Chem. Soc.* **1989**, *111*, 3496. (b) Han, S.; Czernuszewicz, R. S.; Kimura, T.; Adams, M. W. W.; Spiro, T. G. *J. Am. Chem. Soc.* **1989**, *111*, 3505. (c) Fu, W.; Drozdzewski, P. M.; Davies, M. D.; Sligar, S. G.; Johnson, M. K. *J. Biol. Chem.* **1992**, *267*, 15502–15510.

(30) Backes, G.; Mino, Y.; Loehr, T. M.; Meyer, T. E.; Cusanovich, M. A.; Sweeney, W. V.; Adman, E. T.; Sanders-Loehr, J. *J. Am. Chem. Soc.* **1991**, *113*, 2055.

(31) Meyer, J.; Gagnon, J.; Sieker, L. C.; van Dorsselaer, A.; Moulis, J.-M. *Biochem. J.* **1990**, *271*, 839.

(32) Czernuszewicz, R. S.; Nakamoto, K.; Strommen, D. P. *J. Am. Chem. Soc.* **1982**, *104*, 1515.

at 317 cm^{-1} and is flanked by components of the $\nu(E_u)$ Ni–S stretching mode at 362 and 353 cm^{-1} (split due to overall D_{2h} symmetry for the complex anion) and the $\nu(B_{2g})$ mode at 207 cm^{-1}. Since this is a centrosymmetric molecule, only the A_{1g} and B_{2g} modes are observed in the Raman spectrum and the abnormally large frequency separation between these modes is a consequence of differential mixing with deformation motions of the chelate rings. By analogy, for Ni(II)-desulforedoxin, we assign the bands at 327 and 345 cm^{-1} to components of the $\nu(E_u)$ Ni–S stretching mode and the bands at 221 and 288 cm^{-1} to $\nu(B_{2g})$ and $\nu(A_{1g})$ Ni–S stretching modes, respectively. The splitting and Raman intensity of the $\nu(E_u)$ Ni–S stretching mode result from distortions which remove the inversion center from the approximately square planar NiS_4 core.

Out-of-plane bending modes will have very small polarizability changes and hence are expected to be very weak in the Raman spectrum. Hence the lower energy bands at 124, 136, and 170 cm^{-1} are tentatively assigned to the $\delta(E_u)$ and $\delta(B_{1g})$ S–Ni–S in-plane bending modes, although Ni–S–C_β bending is an alternative possibility for the 170-cm^{-1} band. The very weak bands centered at 405 and 440 cm^{-1} may result primarily from deformations of coordinated cysteine residues. However, the weak enhancement of such modes compared to Ni(II)-rubredoxin suggests Ni–S–C_β–C_α dihedral angles close to 90 or 270° in Ni(II)-desulforedoxin.

While these assignments await confirmation in the form of Ni-isotope shifts, the Raman spectrum is clearly consistent with a distorted square planar arrangement of cysteinyl S in Ni(II)-desulforedoxin. In the absence of additional axial ligands this would result in a diamagnetic ($S = 0$) Ni(II) center. However, recent variable-temperature MCD studies have shown that the Ni(II) is paramagnetic ($S = 1$) and that the ground- and excited-state properties are consistent with a five-coordinate Ni(II) center with approximate square pyramidal geometry.[33] The MCD results together with the Raman data suggest that the anomalous arrangement of cysteine residues in desulforedoxin enables nickel to adopt an approximately square planar geometry for the $[NiS_4]$ unit and that this results in the binding of an axial water molecule or additional protein ligand. Since X-ray absorption studies have raised the possibility of a square planar $[NiS_4]$ unit in CO dehydrogenase from *Clostridium thermoaceticum*,[2a,b] Ni(II)-desulforedoxin may serve as a useful biological model system for the nickel center in this enzyme.

(33) Huang, Y.-H.; Moura, I.; LeGall, J.; Moura, J. J. G.; Johnson, M. K. Unpublished results.

Summary

In general, the results presented above demonstrate the utility of resonance Raman for probing the coordination geometry of Ni(II)–tetrathiolate centers in complexes and proteins via the frequencies and properties of Ni–S vibrations that become enhanced with excitation into S → Ni(II) charge-transfer bands. Square planar versus tetrahedral coordination geometries are readily distinguished, and in the latter case the sign and magnitude of a tetragonal distortion can be assessed. More specific conclusions are summarizes as follows: 1. Resonance Raman spectra indicate tetragonally elongated tetrahedral $[NiS_4]$ cores for the $[Ni(SPh)_4]^{2-}$ anion in solution and for Ni(II)-rubredoxins. 2. Although the nature of the cation determines the sign and magnitude of the tetragonal distortion within the $[Ni(SPh)_4]^{2-}$ anion in the crystalline state, the solution resonance Raman studies show that a tetragonally distorted $[NiS_4]$ core is an intrinsic property of this anion, as opposied to a crystal packing effect. 3. As is the case for blue copper proteins, cysteinyl deformation modes that become enhanced via coupling with M–S stretching modes are observed at around 400 cm^{-1} in both native and Ni(II)-rubredoxins. While more work needs to be done on structurally characterized systems, it is clear that resonance Raman provides an effective probe of the conformation of coordinating cysteine residues. 4. Resonance Raman studies suggest an approximately square planar $[NiS_4]$ core in Ni(II)-desulforedoxin.

These studies provide a foundation for using resonance Raman spectroscopy to probe the coordination geometry and cysteine conformation of Ni centers in hydrogenases and CO dehydrogenases and in other Ni(II)-substituted metalloproteins and metalloenzymes. In the case of hydrogenases and CO dehydrogenases, the presence of multiple Fe–S clusters complicates the interpretation of resonance Raman data. However, studies are in progress and resonance Raman spectra of these Ni enzymes and Ni(II)-substituted azurin and liver alcohol dehydrogenase will be the subject of future publications.

Acknowledgment. This work was supported by grants from the NSF (DMB8921986 to M.K.J. and DMB9105150 to M.W.W.A.) and by the NSF Research Training Group Award to the Center for Metalloenzyme Studies (DIR9014281). We thank Professors Stephen Koch and Michelle Millar for useful discussions on the structures of Ni(II) tetrathiolate complexes.